
GradINN: Gradient Informed Neural Network

Filippo Aglietti^{1,2} Francesco Della Santa³ Andrea Piano¹ Virginia Aglietti⁴

¹Energy Department, Politecnico di Torino, Torino, Italy

²Dumarey Automotive Italia S.p.A.

³Department of Mathematical Sciences, Politecnico di Torino, Torino, Italy

⁴Independent Researcher

filippo.aglietti@studenti.polito.it

francesco.dellasanta@polito.it

andrea.piano@polito.it

agliettivirginia@gmail.com

Abstract

We propose Gradient Informed Neural Networks (GradINNs), a methodology inspired by Physics Informed Neural Networks (PINNs) that can be used to efficiently approximate a wide range of physical systems for which the underlying governing equations are completely unknown or cannot be defined, a condition that is often met in complex engineering problems. GradINNs leverage *prior beliefs* about a system's gradient to constrain the predicted function's gradient across all input dimensions. This is achieved using two neural networks: one modeling the target function and an auxiliary network expressing prior beliefs, e.g., smoothness. A customized loss function enables training the first network while enforcing gradient constraints derived from the auxiliary network. We demonstrate the advantages of GradINNs, particularly in low-data regimes, on diverse problems spanning non-time-dependent systems (Friedman function, Stokes Flow) and time-dependent systems (Lotka-Volterra, Burger's equation). Experimental results showcase strong performance compared to standard neural networks and PINN-like approaches across all tested scenarios.

1 Introduction

In the field of computational physics, Neural Networks (NNs) have become an increasingly important tool for modeling complex physical systems that cannot be derived in closed form or for which the traditional empirical models fail to achieve the desired accuracy [19, 6]. Several studies have shown how NNs are powerful function approximators, able to model a wide variety of large, complex, and highly non-linear systems with unprecedented computational efficiency when a large training dataset is available [11, 21, 26, 13]. However, in settings where data is limited or widely dispersed, NNs face considerable difficulties. For instance, in the physical sciences, data is often obtained experimentally and is thus expensive and/or challenging to collect. In such scenarios, NNs show a decreasing prediction performance and a higher probability to overfit to the training data compared to physics white/gray models. On the other hand, the latter suffer from lack of flexibility and expressivity (for instance 0/1-dimensional models) or can require high computational effort as Finite Element Method models [25]. In order to address these difficulties, Physics-Informed Neural Networks (PINNs) emerged in recent years [23]. These models leverage prior knowledge, often in the form of known differential equations (DE), by embedding it directly into the training process. Specifically, they introduce an additional term in the loss function which represents the residual of the underlying DE evaluated on a set of so-called collocation points. This formulation increases robustness against flawed data, e.g., missing or noisy values, and offers physically consistent predictions, particularly in

tasks requiring extrapolation [14]. While PINNs have been shown to perform well across a variety of applications [23, 14, 12, 16, 5, 29, 4, 18] they require *detailed prior knowledge* of the physical system and are thus not directly applicable when this is not available. Recently, PINNs have been extended to deal with various modified settings: systems characterized by *partially unknown* underlying physics [24, 22], unknown data measurement noise [20], gradients observations [27] by using Sobolev training [7] and learning of symplectic gradients (Hamiltonian NNS, [10, 17]).

However, there exists many physical phenomena where the underlying physics is *entirely unknown* or too complex to be easily represented through DES. In those cases it is only possible to rely only on data and *prior beliefs*. GradINNs, gradient informed neural networks, address these settings by differentiating, similarly to PINNs, a primary NN on a set of collocation points. However, differently from PINNs, GradINNs pair the primary network with an auxiliary NN encoding prior belief and leading to an additional loss term which regularizes the predicted solution gradients. As a result, GradINNs can effectively model a broader class of physical systems. In summary, our contributions are as follow:

- We propose GradINN, a simple and efficient technique for training a NN to accurately approximate a function in low data regimes. GradINN constraints the NN’s gradient via an auxiliary network that encodes prior beliefs about the underlying system, and trains both networks via a customized loss that can be easily incorporated into any training pipeline.
- We test GradINNs on a general synthetic function (Friedman) and show how they outperform other NNS, with and without regularization, while being more robust to noisy data.
- We extensively test GradINNs in the context of physical systems. We show how they can be used to learn the solution of ordinary differential equations (ODEs, e.g. Lotka-Volterra system), partial differential equations (PDEs, e.g. Burger’s equation) and systems for which time is not the primary driver of change (Stokes Flow) outperforming NNS across all examples.

2 Preliminaries

Notation We denote by $u(\cdot) : \mathbb{R}^d \rightarrow \mathbb{R}$ a function we aim to model with inputs given by $(t, \boldsymbol{\xi})$, where $t \in \mathbb{R}$ is time and $\boldsymbol{\xi} := [\xi_1, \dots, \xi_{d-1}] \in \mathbb{R}^{d-1}$ is the vector of spatial variables. To avoid cluttering notation we denote $u(\cdot)$ by u hereinafter. Let $u_t := \partial u / \partial t$ be the partial derivative of u with respect to t and $u_{\xi_i} := \partial u / \partial \xi_i$ be the partial derivative of u with respect to the i -th spatial variable ξ_i . Moreover, we denote by $\nabla_{\boldsymbol{\xi}}$ the differential operator that returns the vector of partial derivatives of a function with respect to $\boldsymbol{\xi}$ and with $\nabla_{\boldsymbol{\xi}}^2$ the operator for computing the matrix of second-order partial derivatives with respect to $\boldsymbol{\xi}$. Therefore, $\nabla_{\boldsymbol{\xi}} u := [u_{\xi_1}, \dots, u_{\xi_{d-1}}] \in \mathbb{R}^{d-1}$ and $\nabla_{\boldsymbol{\xi}}^2 u := (u_{\xi_i \xi_j}) = (\partial^2 u / \partial \xi_i \partial \xi_j) \in \mathbb{R}^{(d-1) \times (d-1)}$.

As originally formulated in Raissi [24], PINNs study physical systems governed by a known PDE of the general form:

$$u_t = \mathcal{N}(t, \boldsymbol{\xi}, u, \nabla_{\boldsymbol{\xi}} u, \nabla_{\boldsymbol{\xi}}^2 u, \dots), \quad (1)$$

where \mathcal{N} represents a known potentially nonlinear differential operator that depends on t , on the spatial variables $\boldsymbol{\xi}$, on u and on its derivatives with respect to $\boldsymbol{\xi}$. PINNs approximate the solution u via a NN denoted by $U(\cdot; \Theta) : \mathbb{R}^d \rightarrow \mathbb{R}$ where Θ_U are the network parameters. From Eq. (1) it is possible to define the function $f := u_t - \mathcal{N}(t, \boldsymbol{\xi}, u, \nabla_{\boldsymbol{\xi}} u, \nabla_{\boldsymbol{\xi}}^2 u, \dots)$ and, by plugging in the network U , write:

$$f := U_t(t, \boldsymbol{\xi}; \Theta_U) - \mathcal{N}(t, \boldsymbol{\xi}, U, \nabla_{\boldsymbol{\xi}} U, \nabla_{\boldsymbol{\xi}}^2 U, \dots). \quad (2)$$

where the derivatives $U_t, \nabla_{\boldsymbol{\xi}} U, \nabla_{\boldsymbol{\xi}}^2 U, \dots$ of the network U are computed by automatic differentiation [2]. Given a training dataset $\mathcal{D} = \{(t_n, \boldsymbol{\xi}_n), u_n\}_{n=1}^{N_U}$, including the initial and boundary conditions on u , and a set of collocation points $\mathcal{B} = \{(t_m, \boldsymbol{\xi}_m)\}_{m=1}^M$, the parameters Θ_U can be learned by minimizing the loss function \mathcal{L} defined as:

$$\begin{aligned} \mathcal{L}(\Theta_U) &= \mathcal{L}_U(\Theta_U) + \mathcal{L}_f(\Theta_U) \\ &= \frac{1}{N_U} \sum_{n=1}^{N_U} (U(t_n, \boldsymbol{\xi}_n; \Theta_U) - u_n)^2 + \frac{1}{M} \sum_{m=1}^M (f(t_m, \boldsymbol{\xi}_m; \Theta_U))^2. \end{aligned} \quad (3)$$

The term \mathcal{L}_U constrains the solution u to fit the training data \mathcal{D} whereas \mathcal{L}_f enforces the physics knowledge dictated by Eq. (2) across the set of collocation points \mathcal{B} . The Deep Hidden Physics Models (DHPMs) methodology proposed in [24], similarly to the Universal-PINN (UPINN) approach of [22], extends the PINN formulation to deal with physics problems governed by PDEs (or ODEs) of the form given in Eq. (1) and partially unknown \mathcal{N} . In particular, Raissi [24] considers unknown functional form but known input variables for \mathcal{N} while Podina et al. [22] also assumes partial prior knowledge of the parameters of the functional form. In settings where partial knowledge exists, an auxiliary network $N(\cdot; \Theta_N) : \mathbb{R}^D \rightarrow \mathbb{R}$ is used to approximate \mathcal{N} . Note that the inputs to N (and thus the value of D) are problem specific and correspond to the inputs of \mathcal{N} thus encoding partial knowledge of the system. By plugging N into Eq. (2) we can write:

$$f := U_t(t, \boldsymbol{\xi}; \Theta_U) - N(t, \boldsymbol{\xi}, U, \nabla_{\boldsymbol{\xi}} U, \nabla_{\boldsymbol{\xi}}^2 U, \dots; \Theta_N). \quad (4)$$

In this case, (Θ_U, Θ_N) are learned considering the same \mathcal{L}_U and a modified version of \mathcal{L}_f in which f is given by Eq. (4). The training dataset \mathcal{D} is then augmented to include, in addition to initial and boundary conditions, data points within the domain of u so as to compensate for the lack of prior knowledge of the system governing DES.

In the next section, we illustrate a new approach that is partially inspired by this PINNs formulation, but that addresses cases where the form of Eq. (1) (and as a consequence the form of N) is fully unknown or cannot be defined thus only data and prior beliefs about the system are available.

3 GradINN

The approach we propose in this paper, which we name Gradient Informed Neural Network (GradINN), targets systems of the form $u(\boldsymbol{x}) \in \mathbb{R}^{d_o}$, where $\boldsymbol{x} \in \mathbb{R}^d$ represents all the dimensions of the problem making no distinction between temporal and spatial variables. As done in Section 2, we denote by $\nabla_{\boldsymbol{x}}$ and $\nabla_{\boldsymbol{x}}^2$ the differential operators for the first and second order derivatives with respect to all the dimensions of vector \boldsymbol{x} respectively.¹ We first introduce the methodology for uni-dimensional outputs ($d_o = 1$) and then discuss the extension to multi-output systems ($d_o > 1$).

GradINN deals with systems where the governing equation, i.e., Eq. (1), is unknown or cannot be defined, and only general behaviour for $\nabla_{\boldsymbol{x}} u$ can be assumed. Similar to Eq. (4), GradINN consists of two paired NNS, $U(\cdot; \Theta_U) : \mathbb{R}^d \rightarrow \mathbb{R}$ and $F(\cdot; \Theta_F) : \mathbb{R}^d \rightarrow \mathbb{R}^d$. U is used to approximate u while F , taking \boldsymbol{x} as input and returning the beliefs about $\nabla_{\boldsymbol{x}} u$ as output, is used to apply implicit constraints on $\nabla_{\boldsymbol{x}} U$. In particular, the *initialization* of F encodes general *prior* beliefs on the behavior of $\nabla_{\boldsymbol{x}} u$, e.g., smoothness, and, therefore, of u itself. For instance, F can be initialized to give constant outputs to encourage smoothness in the predicted solution given by U (see below and Fig. 1 for a toy example). Given a training dataset $\mathcal{D}_{\text{TRAIN}} = \{\boldsymbol{x}_n, u_n\}_{n=1}^{N_U}$ and a set of collocation points $\mathcal{C} = \{\boldsymbol{x}_m\}_{m=1}^M$, we train the paired NNS simultaneously by considering the following loss function:

$$\begin{aligned} \mathcal{L}(\Theta_U, \Theta_F) &= \mathcal{L}_U(\Theta_U) + \mathcal{L}_F(\Theta_F; \Theta_U) = \\ &= \mathcal{L}_U(\Theta_U) + \frac{1}{M} \sum_{m=1}^M \|F(\boldsymbol{x}_m; \Theta_F) - \nabla_{\boldsymbol{x}} U(\boldsymbol{x}_m; \Theta_U)\|_2^2 = \\ &= \mathcal{L}_U(\Theta_U) + \frac{1}{M} \sum_{m=1}^M \sum_{i=1}^d (F_i(\boldsymbol{x}_m; \Theta_F) - U_{x_i}(\boldsymbol{x}_m; \Theta_U))^2, \end{aligned} \quad (5)$$

where the first component $\mathcal{L}_U(\Theta_U)$ is defined, similarly to Eq. (3), as $\mathcal{L}_U(\Theta_U) = \frac{1}{N_U} \sum_{n=1}^{N_U} (U(\boldsymbol{x}_n; \Theta_U) - u_n)^2$. Note how \mathcal{L}_U optimizes Θ_U to have $U(\boldsymbol{x}; \Theta_U) \approx u(\boldsymbol{x})$ over $\mathcal{D}_{\text{TRAIN}}$. At the same time, \mathcal{L}_F allows optimizing both Θ_U and Θ_F such that $F(\boldsymbol{x}; \Theta_F) - \nabla_{\boldsymbol{x}} U(\boldsymbol{x}; \Theta_U) \approx \mathbf{0}$ for $\boldsymbol{x} \in \mathcal{C}$. In particular, by updating Θ_U , this loss term encourages U to have a gradient behavior similar to F . Simultaneously, it modifies Θ_F to bring F closer to $\nabla_{\boldsymbol{x}} U$, thereby relaxing the prior beliefs on \mathcal{C} using the gradient information derived from $\mathcal{D}_{\text{TRAIN}}$ via \mathcal{L}_U . As \mathcal{C} does not require access to the output values, it can be increased without the need to collect expensive experimental data but only accounting for the available computation resources or model efficiency considerations. Finally,

¹Note that this notation is adopted to distinguish the NN differentiation with respect to \boldsymbol{x} instead of the model's weights.

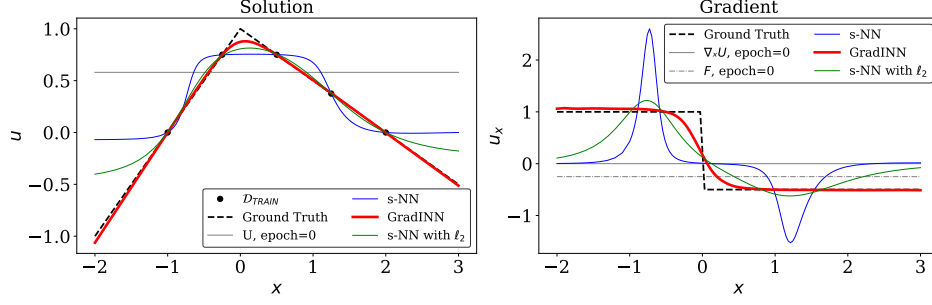


Figure 1: Ground truth (black dashed lines) and predicted solution (left) and gradient (right) both at initialization (gray lines) and after training. Predictions for GradINN are obtained with $M = 100$ collocation points uniformly distributed $[-2, 3]$.

analogously to Eq. (3), the proposed loss can be minimized using backpropagation and off-the-shelf optimizers thus being easily incorporated into any training pipeline.

To further clarify the impact of the proposed loss (Eq. (5)) and shed light of GradINN’s working mechanism, we show a toy example where GradINN, a standard NN² (denoted by s-NN henceforth), and a s-NN with ℓ_2 -regularisation are trained on a simple system $u : [-2, 3] \rightarrow \mathbb{R}$, ($d=1$, $d_o=1$), using $N_U = 5$ training points. Fig. 1 shows the ground truth solution (left, black line) and gradient (right, black line) together with $\mathcal{D}_{\text{TRAIN}}$ (black dots) and the predictions both at initialization (gray lines); note that the initialization of U is the same for s-NN, s-NN with ℓ_2 and GradINN) and after training. Notice how, initializing U and F in a way that corresponds to smooth predictions (constant in these plots) for both the solution and its gradient, leads GradINN to accurately predict u within the training domain $[-1, 2]$ (left plot). Similar results are obtained with a s-NN with ℓ_2 . This is the result of gradient regularization which can be appreciated by looking at the right plot and noticing how both GradINN and the s-NN with ℓ_2 better fit the ground truth gradient respect to s-NN. However, while ℓ_2 induces a reduction in the gradient’s magnitude, it does not prevent it from oscillating, see green curve behaviour with respect to the black dashed line on the input space boundaries (around $x < -1$ and $x > 2$). Instead, GradINN reduces the magnitude of the gradient but also penalises its oscillations via the term \mathcal{L}_F . A similar behaviour is observed when initializing U to have less smooth predictions for u but keeping the initialization of F unchanged, see Fig. 7 (top row). On the contrary, initializing F to give less smooth predictions, leads GradINN to converge to a less smooth solution (Fig. 7, bottom row) in line with the interpretation of F as expressing prior beliefs. See Appendix A for further details.

Higher order derivatives GradINN can be easily extended to incorporate constraints on higher-order derivatives. For instance, we can constrain the second order derivatives by introducing a third network, $G(\cdot, \Theta_G) : \mathbb{R}^d \rightarrow \mathbb{R}^{d \times d}$ and considering the augmented loss $\mathcal{L}(\Theta_U, \Theta_F, \Theta_G) = \mathcal{L}_U(\Theta_U) + \mathcal{L}_F(\Theta_U, \Theta_F) + \mathcal{L}_G(\Theta_U, \Theta_G)$ where \mathcal{L}_G is given by:

$$\mathcal{L}_G(\Theta_U, \Theta_G) = \frac{1}{M} \sum_{m=1}^M \sum_{i,j=1}^d (G_{ij}(\mathbf{x}_m; \Theta_G) - U_{x_i x_j}(\mathbf{x}_m; \Theta_U))^2 \quad (6)$$

with G_{ij} giving the (i, j) -output of the second auxiliary network and $U_{x_i x_j}$ representing the second order partial derivative of U with respect to x_i and x_j . An equivalent formulation can be written by using a unique network F with increased output dimension but still considering an additional loss component for each gradient order to be constrained.

Multi-outputs system Finally, GradINNs can also be used to approximate multi-output systems in which $u(\cdot) : \mathbb{R}^d \rightarrow \mathbb{R}^{d_o}$. In this setting, we have $U(\cdot; \Theta_U) : \mathbb{R}^d \rightarrow \mathbb{R}^{d_o}$ and $F(\cdot; \Theta_F) : \mathbb{R}^d \rightarrow \mathbb{R}^{d \times d_o}$

²Here and in the rest of the paper, we call standard NN a NN trained only with \mathcal{L}_U on $\mathcal{D}_{\text{TRAIN}}$.

and write \mathcal{L}_U and \mathcal{L}_F as follow:

$$\mathcal{L}_U(\Theta_U) = \frac{1}{N_U} \sum_{n=1}^{N_U} \sum_{k=1}^{d_o} (U^k(\mathbf{x}_n; \Theta_U) - u_n^k)^2, \quad (7)$$

$$\mathcal{L}_F(\Theta_F, \Theta_U) = \frac{1}{M} \sum_{m=1}^M \sum_{i=1}^d \sum_{k=1}^{d_o} (F_i^k(\mathbf{x}_m; \Theta_F) - U_{x_i}^k(\mathbf{x}_m; \Theta_U))^2. \quad (8)$$

where U^k and u_n^k are the k -th network and ground truth output respectively, $U_{x_i}^k$ is the derivative of the k -th output with respect to the i -th input and F_i^k is the corresponding output of the auxiliary network.

4 Experiments

We test GradINNs on a well known synthetic function, that is the Friedman function (FRIEDMAN, $d = 5$, $d_o = 1$), and three physical systems featuring different characteristics in terms of time dependency, input and output dimension and smoothness of the gradients:

- the Stokes Flow (STOKES), which can be used to describe the motion of fluids around a sphere, in conditions of low Reynolds number ($Re < 1$). In this experiment $d_o = 1$, there is no dependency of u on time and $d = 2$.
- The Lotka-Volterra system (LV), an ODE model of predator-prey dynamics in ecological systems. This system’s u depends on time, which is the only input ($d = 1$), and $d_o = 2$.
- The Burger’s equation (BURGER), a challenging PDE studied in fluid mechanics to represents shock waves and turbulence. In this case u depends on time and a spatial variable ($d = 2$) and $d_o = 1$. This equation is particularly challenging due to steep partial derivatives within the solution’s domain.

Metrics Given a test dataset $\mathcal{D}_{\text{TEST}} = \{\mathbf{x}_h, u_h\}_{h=1}^{N_{\text{TEST}}}$, GradINN’s performance is assessed in terms of root mean squared error of both output (RMSE $_U$ ³) and gradient predictions (RMSE $_{\partial}$ ⁴). In order to compute RMSE $_{\partial}$, we derive the ground truth gradient analytically via closed-form differentiation of the original function (for FRIEDMAN) or through the ODE (for LV). When analytical computation of the gradient is not possible, this is obtained via automatic differentiation of a standard NN that has been trained on a large dataset ($N_U > 10^4$) to ensures accurate predictions for both the solution and its gradient (for STOKES and BURGER).

Baselines As GradINN does not rely on prior physical knowledge, we mainly compare it against s-NNs. However, for completeness of our experimental results, we also report figures obtained with Sobolev training [7] (denoted by ST henceforth), UPINN and DHPM despite these models assume a certain level of prior knowledge of the governing equations and its gradient. In particular, ST assumes the availability of a training dataset that also includes the ground truth values of the gradient for each $\mathbf{x} \in \mathcal{D}_{\text{TRAIN}}$. DHPM assumes known inputs of the auxiliary network N (see Eq.(4)). Finally, UPINN assumes, on top of the inputs of N , partial knowledge of the functional form of \mathcal{N} . Note that, for both UPINN and DHPM, we do not re-run the code associated to these two methodologies but use the figures reported in the corresponding papers [24, 22] directly.

Experimental details The network architectures of both U and F are fixed across all experiments. In particular, we set U to be a network with three hidden layers including 20 neurons each. For F we consider two hidden layers comprising 50 neurons each. Both U and F use sigmoid activation functions across all layers except the final one, which employs a linear activation function. U and F are trained simultaneously for 10^4 epochs. For U , a fixed batch size (bs_U) of 64 is used for all experiments apart from LV where $bs_U = 5$. For F , the batch size bs_F is set according to $bs_F = bs_U \times M/N_U$. The s-NN used for comparison uses the same network architecture for U and is

³RMSE $_U = \sqrt{\frac{1}{N_{\text{TEST}}} \sum_{h=1}^{N_{\text{TEST}}} (U_h - u_h)^2}$ where u_h and U_h are the ground truth solution and GradINN’s predicted output for the h -th datapoint \mathbf{x}_h in $\mathcal{D}_{\text{TEST}}$ respectively.

⁴RMSE $_{\partial} = \sqrt{\frac{1}{N_{\text{TEST}}} \sum_{h=1}^{N_{\text{TEST}}} (U_{x_i,h} - u_{x_i,h})^2}$ where $U_{x_i,h}$ and $u_{x_i,h}$ are GradINN’s gradient prediction and the ground truth gradient with respect to the i -th dimension x_i of a given test point \mathbf{x}_h respectively.

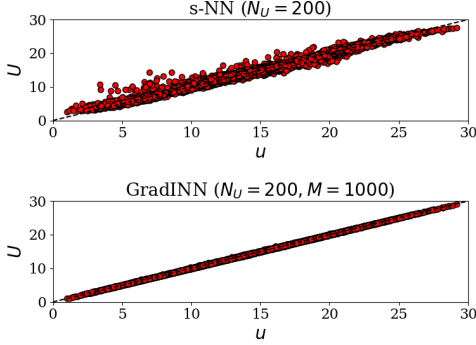


Figure 2: FRIEDMAN. Predicted output U vs u for each $\mathbf{x}_n \in \mathcal{D}_{\text{TEST}}$. *Top:* s-NN with $\text{RMSE}_U = 0.51$. *Bottom:* GradINN with $\text{RMSE}_U = 0.04$.

Table 1: FRIEDMAN. RMSE_U for different values of N_U and M when $\sigma^2 = 0$. For each value of N_U the lowest RMSE is bolded.

		N_U			
		50	100	200	500
s-NN	-	2.24	1.55	0.51	0.02
	ℓ_1	1.48	0.61	0.13	0.05
	ℓ_2	1.52	0.48	0.13	0.06
GradINN	$M = 500$	0.77	0.24	0.07	0.02
	$M = 10^3$	0.75	0.22	0.04	0.02
	$M = 10^4$	0.66	0.19	0.05	0.02
ST		1.50	0.50	0.17	0.02

Table 2: FRIEDMAN. RMSE_∂ for different values of N_U and across input dimensions when $\sigma^2 = 0$.

N_U	s-NN					GradINN ($M = 10^3$)					ST				
	U_{x_1}	U_{x_2}	U_{x_3}	U_{x_4}	U_{x_5}	U_{x_1}	U_{x_2}	U_{x_3}	U_{x_4}	U_{x_5}	U_{x_1}	U_{x_2}	U_{x_3}	U_{x_4}	U_{x_5}
50	10.30	9.50	11.10	5.88	3.99	3.68	4.44	3.84	0.71	0.69	7.60	8.20	7.90	3.40	3.30
100	7.30	7.80	8.20	5.30	4.33	1.83	1.90	0.45	0.25	0.10	3.50	3.50	2.60	1.40	1.30
200	3.97	3.66	3.35	2.07	1.74	0.44	0.48	0.42	0.09	0.05	2.10	2.30	1.01	0.72	0.39
500	0.29	0.25	0.30	0.1	0.05	0.22	0.21	0.15	0.03	0.02	0.52	0.30	0.20	0.10	0.05

trained for the same number of epochs. We use Adam optimizer [15] with a learning rate determined by an inverse time decay schedule, where the learning rate starts at 0.1 and continuously decreases over 500 epochs based on a decay rate of 0.90. Across all experiment, both U and F are initialized with biases set to zero and weights with *Glorot uniform* distribution (see [9]). This leads to constant network outputs (for both U and F) at initialization which imply smooth prior beliefs.⁵

4.1 FRIEDMAN

In this section we assess GradINN’s performance on the five dimensional Friedman function [8]:

$$u(\mathbf{x}) = 10 \sin(\pi x_1 x_2) + 20(x_3 - 0.5)^2 + 10x_4 + 5x_5 + \epsilon \quad (9)$$

where $\epsilon \sim \mathcal{N}(0, \sigma^2)$ with σ^2 taking different values across experiments. We construct $\mathcal{D}_{\text{TRAIN}}$ and \mathcal{C} by sampling input points (via Latin hypercube sampling) in the 5-dimensional unit hypercube and obtaining the corresponding output values via Eq. (9). The test dataset includes $N_{\text{TEST}} = 10^4$ points uniformly sampled in the 5-dimensional unit hypercube. We first demonstrate our approach on noise-free data ($\sigma^2 = 0$) and then explore settings with increasing level of σ^2 .

We compare GradINN with varying number M of collocation points against s-NN, s-NN with ℓ_1 and ℓ_2 regularization⁶ and ST, despite the different training dataset considered by the latter. Table 1 and Table 2 show the RMSE performances achieved in the noiseless data case ($\sigma^2 = 0$) for the output and gradient predictions respectively and across different values of N_U (RMSE $_\partial$ for s-NN with ℓ_1 and ℓ_2 regularization are reported in Table 6 in the appendix). Notice how, for a fixed value of N_U , GradINN significantly outperforms s-NN in terms of output predictions both with and without regularization (see Fig. 2 for a visualization of the difference between the ground truth and the predicted output values over the test dataset). As expected, the use of an increasing M further decreases the RMSE $_U$ in settings where N_U is low. In addition, note how GradINN outperforms ST without having access to the true gradient values for the training points. More importantly, GradINN displays high performance in terms of gradient predictions across all input dimensions and

⁵All experiments were performed on a local machine with 6 CPUs (2.10GHz, 16GB of RAM).

⁶We choose ℓ_1 and ℓ_2 values to be those giving the lower RMSE $_U$ values over $\mathcal{D}_{\text{TEST}}$. The figures shown are thus a lower bound on the RMSE achieved with ℓ_1 or ℓ_2 regularization. Note that considering ℓ_1 or ℓ_2 for $N_U = 500$ leads to increased RMSE.

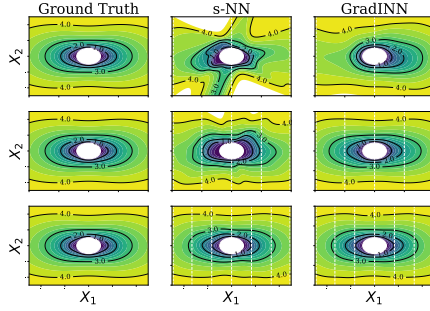


Figure 4: STOKES. Predicted solution and ground truth values (first column) for different N_U values (white dotted lines). *Top:* $N_U = 350$. *Middle:* $N_U = 550$. *Bottom:* $N_U = 750$.

Table 3: STOKES. RMSE_U and RMSE_∂ for different N_U . For each N_U , the lowest RMSE values are bolded.

		N_U		
		350	550	750
U	s-NN	0.37	0.20	0.04
	GradINN	0.24	0.05	0.03
U_{x_1}	s-NN	0.51	0.31	0.09
	GradINN	0.27	0.09	0.05
U_{x_2}	s-NN	0.44	0.32	0.08
	GradINN	0.17	0.07	0.07

all settings of N_U (Table 2). This can be further appreciated by looking at Fig. 8 in the appendix which shows the gradient prediction $\nabla_{\mathbf{x}}U$ for both s-NN and GradINN. As expected, when $\mathcal{D}_{\text{TRAIN}}$ is sufficient to characterize the system (N_U is high) the performance of s-NN matches the one achieved by GradINN both in terms of RMSE_U and RMSE_∂ . When instead $M = 0$, GradINN simplifies ($\mathcal{L}_F = 0$) thus approaching s-NN.

We repeat the same analysis with fixed values of $N_U = 200$ and $M = 1000$ but an increasing level of noise in $\mathcal{D}_{\text{TRAIN}}$. Denote by σ_u the standard deviation of the output values in the $\mathcal{D}_{\text{TRAIN}}$ and let c be a constant taking values in $[0.01, 0.03, 0.05]$. We set $\epsilon \sim \mathcal{N}(0, (c\sigma_u)^2)$ so as to make the noise proportional to the variability of the output values thus simulating real-world data imperfections and testing the GradINN’s robustness. Although all models exhibit a decreasing performance for increasing c , GradINN demonstrates higher accuracy across all noise levels thus being more robust to e.g. measurement errors (Table 7 in Appendix C).

4.2 STOKES

Next, we test our proposed methodology on the Stokes flow [28], also known as creeping flow or viscous flow. This regime describes fluid motion at very low Reynolds numbers, where inertial forces are negligible compared to viscous forces. In the case of a sphere of radius R (white circle in Fig. 4) moving through a fluid with relative far-field velocity \hat{u}_∞ , the Stokes flow permits a closed-form solution $u(\mathbf{x}) \in \mathbb{R}^3$ at any point $\mathbf{x} = [x_1, x_2, x_3]^T$. Denote by $\mathbf{x} \otimes \mathbf{x}$ the tensor product of \mathbf{x} with itself, by $\|\mathbf{x}\|$ the Euclidean norm of \mathbf{x} and by \mathbf{I} the identity matrix, the Stoke flow is defined as:

$$u(\mathbf{x}) = \left(\frac{3R^3 \mathbf{x} \otimes \mathbf{x}}{4 \|\mathbf{x}\|^5} - \frac{R^3 \mathbf{I}}{4 \|\mathbf{x}\|^3} - \frac{3R \mathbf{x} \otimes \mathbf{x}}{4 \|\mathbf{x}\|^3} - \frac{3R \mathbf{I}}{4 \|\mathbf{x}\|} + \mathbf{I} \right) \times \hat{u}_\infty.$$

We reduce the input dimension for \mathbf{x} to $d = 2$ by fixing $x_3 = 0$ and considering input values, for both x_1 and x_2 , in $[-5, 5]$. Similarly, we reduce the output dimension to one by taking the Euclidean norm $\|\mathbf{u}\|$ of each output vector and training both GradINN and s-NN on those. We fix $\hat{u}_\infty = [5, 0, 0]^T$. We generate $\mathcal{D}_{\text{TRAIN}}$ by considering a regular grid of input values of size $N_U \in [300, 500, 700]$ (see dotted white lines in Fig. 4). As the homogeneous Dirichlet boundary conditions are assumed to be known, we add 50 points along the sphere’s perimeter section with $\|\mathbf{u}\| = 0$ to this training dataset. \mathcal{C} is constructed by taking $M = 10^4$ points in the $[-5, 5]^2$ domain. Similarly, $\mathcal{D}_{\text{TEST}}$ includes a regular grid of points $N_{\text{TEST}} = 4 \times 10^4$ in the same domain. GradINN outperforms s-NN across all N_U values, both in terms of output and gradients predictions

$$^7 \|\mathbf{u}\| = \sqrt{u_1^2 + u_2^2 + \dots + u_n^2} \text{ for } \mathbf{u} = (u_1, u_2, \dots, u_n).$$

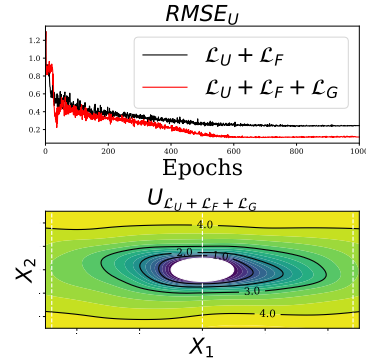


Figure 3: STOKES. *Top:* RMSE_U over training epochs when constraining $\nabla_{\mathbf{x}}U$ (black line) and both the $\nabla_{\mathbf{x}}U$ and $\nabla_{\mathbf{x}}^2U$ (red line). *Bottom:* predicted solution when constraining $\nabla_{\mathbf{x}}U$ and $\nabla_{\mathbf{x}}^2U$ ($N_U = 350$).

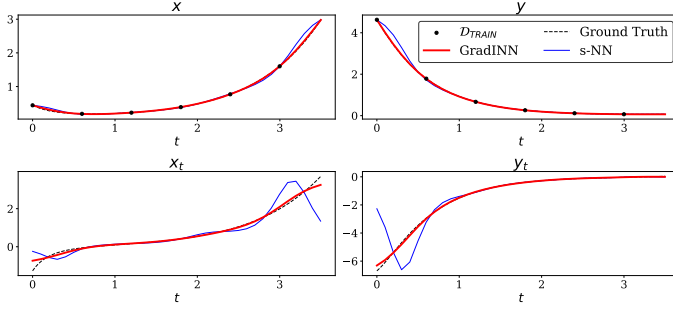


Figure 5: LV. *Top:* Predicted solution. *Bottom:* Predicted gradient.

Table 4: LV. RMSE_∂ for the predator’s uptake functions i.e. $-\beta xy$ and δxy , the lowest RMSE values are bolded.

Method		RMSE
UPINN	-	0.03
s-NN	$-\beta xy$	0.11
	δxy	0.16
GradINN	$-\beta xy$	0.03
	δxy	0.025

(Table 3). In particular, s-NN exhibits a behaviour similar to the ground truth solution only when trained with $N_U = 750$ (Fig. 4, bottom row). On the contrary GradINN successfully reconstructs the ground truth solution starting from $N_U = 550$ (see Fig. 4, middle and bottom rows).

We further test GradINN by applying the loss given in Eq. (6) to constrain both $\nabla_x U$ and $\nabla_x^2 U$. We fix $N_U = 350$ and keep the same \mathcal{C} . Fig. 3 (top) shows how incorporating the additional \mathcal{L}_G decreases RMSE_U (from 0.24 to 0.11) leading to a predicted solution (Fig. 3, bottom) closer to the ground truth (see first col of Fig. 4). This further highlights the benefit and flexibility of the proposed methodology. The same procedure was followed for $N_U = 550$ and $N_U = 750$ but given the already high accuracy of GradINN reached with these sizes of $\mathcal{D}_{\text{TRAIN}}$ using only $\mathcal{L}_U + \mathcal{L}_F$, no significant further improvement was observed in terms of both RMSE_U and RMSE_∂ when constraining the second order gradient. Note that, although the RMSE_U stabilises within 1000 epochs in both configurations (Fig. 3, top), the computational effort significantly increases when constraining the second-order gradient leading to higher training time.

4.3 LV

Moving to time-dependent systems, we test GradINN on the Lotka-Volterra (LV) system [3], described by the following ODEs:

$$x_t = \alpha x - \beta xy \quad y_t = \delta xy - \gamma y, \quad (10)$$

where x and y represent the populations of two species, typically prey and predators respectively. The parameters α and β characterize the prey dynamics while γ and δ characterize the predator dynamics. As in Podina et al. [22], we numerically solve the system for $[\alpha, \beta, \gamma, \delta] = [1.3, 0.9, 0.8, 1.4]$ with initial condition $[x_0, y_0] = [0.44249296, 4.6280594]$ and exploit the solution to generate $\mathcal{D}_{\text{TRAIN}}$ with $N_U = 5$ and uniformly distributed input values in $t \in [0, 3]$. For GradINN we set $M = 1000$. GradINN gives more accurate predictions compared to s-NN, both in terms of the predicted output (Fig. 5, top) and gradients (Fig. 5, bottom). We compare the gradient predictions obtained with GradINN against the results reported in [22], where UPINN is used to discover only part of the system in Eq. (10), namely the predator’s uptake functions, i.e., $-\beta xy$ and δxy . Using the same $\mathcal{D}_{\text{TRAIN}}$ and number of collocation points ($M = 1000$), UPINN achieves an average RMSE_∂ across the unknown parts of the gradients of 0.03^8 . Instead, GradINN’s average RMSE_∂ across output dimensions is 0.08. The difference in these RMSE values can be attributed to the absence of prior knowledge considered by GradINN. Indeed, this value of RMSE_∂ also includes the predictions for the parts of Eq. (10) that are considered known in UPINN. To facilitate the comparison of GradINN and UPINN and have a more comparable metric, we evaluate the RMSE_∂ only for the predator’s uptake functions (Table 4). In this case, GradINN prediction accuracy over $-\beta xy$ and δxy is comparable to the one achieved by UPINN.

4.4 BURGER

Finally, we test GradINN’s capability to solve PDEs by considering the Burgers’ equation [1]. For a given field $u(t, x)$ and kinematic viscosity ν this is defined as $u_t + uu_x = \nu u_{xx}$. We consider the initial conditions $u(0, x) = -\sin(\pi x/8)$ with $x \in [-8, 8]$, $t \in [0, 10]$, $\nu = 0.1$ and known Dirichlet boundary conditions. We take the solutions of the PDE from [24]. This gives a set of 201×256

⁸It is not clear how the RMSE of the predictions for $-\beta xy$ and δxy is computed in [22].

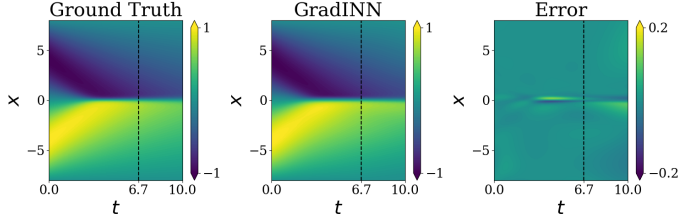


Figure 6: BURGER. *Left:* Ground truth solution. *Middle:* GradINN’s predicted solution. *Right:* Difference between GradINN solution and ground truth values. Using $\mathcal{D}_{\text{TRAIN}}$ in $t \in [0, 6.7]$ (left of black line), GradINN gives $\text{RMSE}_U = 0.02$, $\text{RMSE}_{U_t} = 0.04$ and $\text{RMSE}_{U_x} = 0.02$.

Table 5: BURGER. \mathcal{L}_2^r for GradINN, s-NN, and DHPM with (DHPM⁺) and without (DHPM⁻) prior knowledge on \mathcal{N} ’s inputs. The lowest RMSE values is bolded.

Method	\mathcal{L}_2^r
s-NN	11×10^{-2}
GradINN	2.7×10^{-2}
DHPM ⁺	0.48×10^{-2}
DHPM ⁻	1.46

points from which we select $N_U = 1000$ for $\mathcal{D}_{\text{TRAIN}}$ in $t \in [0, 6.7]$ and keep the rest for $\mathcal{D}_{\text{TEST}}$. Note that we select $\mathcal{D}_{\text{TRAIN}}$ to cover approximately two-thirds of the complete input domain thus testing the model capability to generalize outside of the training domain. To construct \mathcal{C} , we uniformly sample $M = 22000$ points in the full inputs domain.

GradINN’s predicted solution, along with the ground truth values and the difference between these two are given in Fig. 6. This comparison reveals a slight oversmoothing of GradINN’s predicted solution near the steep gradient at $x = 0$, resulting in a localized increase in error (Fig. 6, right).⁹ To directly compare our results against the DHPM figures given in [24], we compute an alternative metric that is the relative \mathcal{L}_2 (\mathcal{L}_2^r) error.¹⁰ As in the previous experiments, GradINN outperforms s-NN (Table 5) while, as expected, the DHPM approach using prior knowledge (DHPM⁺) achieves a higher accuracy. However, it is important to note that, as reported in [24], this performance depends on the knowledge of the input variables for \mathcal{N} (see Eq. (4)). When the prior knowledge of which variables influence the system’s dynamics is removed (DHPM⁻), \mathcal{L}_2^r increases up to 1.46 thus performing significantly worse than GradINN.

5 Conclusions and discussion

We introduced GradINN, a general methodology for training NN that (i) allows regularizing gradient of different orders using prior beliefs, (ii) does not require prior knowledge of the system and (iii) can be used across setting where input and output have different dimensions. Our extensive experimental comparison showed how GradINN can be used to accurately predict the behaviour of various physical systems in sparse data conditions. In particular, GradINN outperforms s-NN and performs similarly to PINN-like approaches by only using data and prior beliefs.

Limitations In this work we focused on physical systems and consider smooth networks’ initializations. However, this might not be the optimal initialization for problems that exhibit local discontinuities or regions with very steep gradients. For example, as shown for BURGER (Fig. 6 and 9), a smooth initialization can lead oversmooth predictions in areas where the solution is very steep. This highlights the need to define more complex priors to handle such conditions, as well as an effective way to embed such priors in the network F (e.g., dedicated pretraining of the auxiliary network F). Additionally, GradINN incurs a higher computational cost compared to s-NN. Indeed, in addition to the standard forward and backward propagation required to update the weights of the networks, GradINN needs to differentiate the network to evaluate the gradient $\nabla_x U$ which translates into a higher computational cost.

Future Work This work opens up several promising avenues for future research. First, different variations of the proposed loss $\mathcal{L}(\Theta_U, \Theta_F)$ could be considered. For instance, one could use a weighted sum of \mathcal{L}_U and \mathcal{L}_F with hyperparameters multiplying the two losses thus prioritizing training data vs prior beliefs (or viceversa). The loss could also be further modified to incorporate a consistency loss as discussed in Appendix B. Finally, more work is needed to understand the impact

⁹To further analyze this phenomenon, we run an additional experiment with $\nu = 0.01/\pi$, a configuration that leads to even steeper gradient, and observed a more pronounced oversmoothing, see Appendix D.

¹⁰ $\mathcal{L}_2^r = \sqrt{\frac{\sum_{h=1}^{N_{\text{TEST}}} (u_h - U_h)^2}{\sum_{h=1}^{N_{\text{TEST}}} u_h^2}}$ where u_h and U_h give the ground truth and predicted value for \mathbf{x}_h respectively.

of non-smooth F initialization, as well as more complex prior beliefs such as highly oscillatory behaviors or discontinuities. This will further enhance the flexibility and applicability of GradINN in modeling a broader range of complex systems.

A Different network initializations

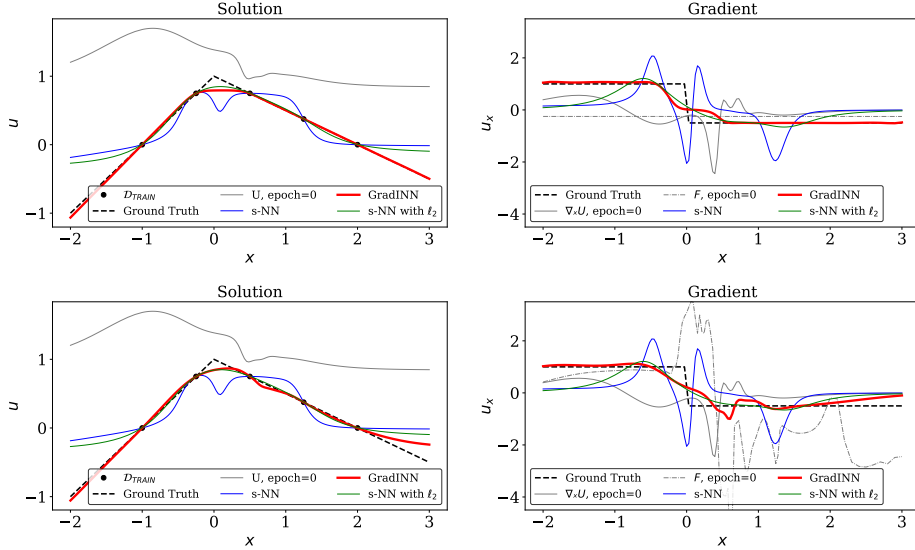


Figure 7: Ground truth (black dashed lines) and predicted solution (left) and gradient (right) at initialization (gray lines) and after training. Predictions for GradINN are obtained with $M = 100$ collocation points uniformly distributed $[-2, 3]$. *Top row:* Non-smooth initialization of U and smooth initialization of F . *Bottom row:* Non-smooth initialization of both U and F .

We repeat the experiment shown in Fig. 1 using a different initialization for both U and F to clarify the impact of a non-smooth initializations. We first consider a non-smooth initialization of U but a smooth initialization of F (top row of Fig. 7). In this setting, s-NN converges to a very wiggly solution (blue curve) that improves within the interval $[-1, 2]$ when considering the l_2 norm. When GradINN is used, similarly to Fig. 1, the smoothness of F allows recovering a smoother solution with fewer oscillations (red line). When instead the F initialization is less smooth (dotted grey line in the bottom row of Fig. 7), GradINN recover a less smooth prediction. This is in line with our interpretation of the auxiliary network as expressing prior beliefs.

B Additional loss term

Considering the formulation given in Section 3 for the higher order derivatives, we can embed the second order derivatives with further information adding a consistency loss among the networks F and G . In particular, given that F represents the prior belief on the behaviour of $\nabla_x u$ and G represent the prior belief on the behaviour of $\nabla_x^2 u$, we can consider the following additional loss term that allows minimizing the residual between G and the first-order derivative of F :

$$\mathcal{L}_{GF}(\Theta_G, \Theta_F) = \frac{1}{M} \sum_{m=1}^M \sum_{i,j=1}^d \left(G_{ij}(\mathbf{x}_m; \Theta_G) - F_{x_j}^i(\mathbf{x}_m; \Theta_F) \right)^2. \quad (11)$$

The investigation of the effect of this additional loss term will be part of future work.

C Additional results for FRIEDMAN

See Figure 8 for additional results.

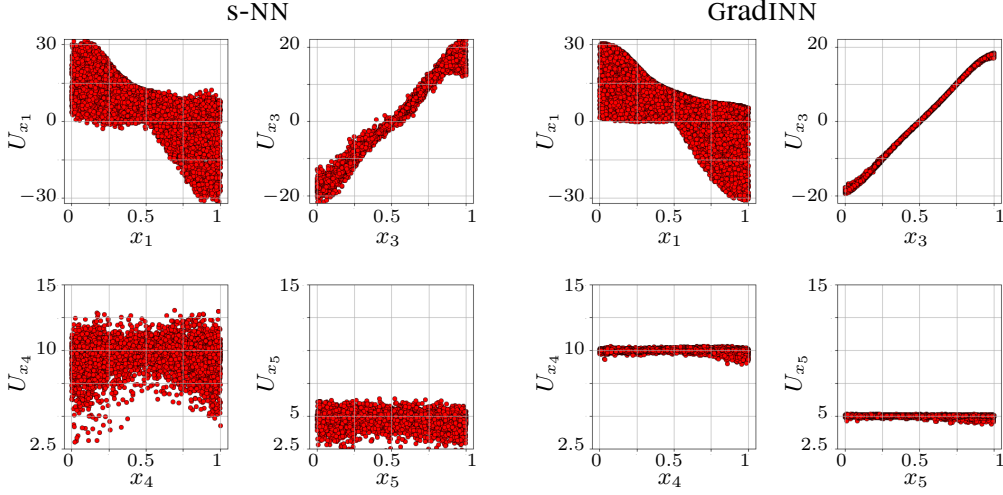


Figure 8: FRIEDMAN. *Left two columns:* s-NN with $n = 200$ ($\text{RMSE}_U = 0.51$). *Right two columns:* GradINN with $n = 200$ and $m = 1000$ ($\text{RMSE}_U = 0.04$). The plot shows the learned gradient U_{x_i} for each dimension $x_i, i = 1, \dots, 5$ and point $\mathbf{x}_n \in \mathcal{D}_{\text{TEST}}$ (U_{x_2} is not reported as similar to U_{x_1}).

Table 6: FRIEDMAN. RMSE_θ for different values of N_U and across input dimensions when $\sigma^2 = 0$.

N_U	s-NN with ℓ_1					s-NN with ℓ_2				
	U_{x_1}	U_{x_2}	U_{x_3}	U_{x_4}	U_{x_5}	U_{x_1}	U_{x_2}	U_{x_3}	U_{x_4}	U_{x_5}
50	6.1	6.5	8	3.0	2.6	5.9	6.0	7.9	2.9	2.28
100	3.9	3.7	2.8	1.27	0.9	3.2	3.1	2.0	1.1	0.67
200	1.1	1.0	1.1	0.5	0.3	1.3	1.1	0.85	0.44	0.25
500	0.6	0.63	0.40	0.22	0.07	0.59	0.58	0.52	0.21	0.11

D Additional results for BURGER

To further analyze the phenomenon of solution oversmoothing shown in Fig.6, we repeated the BURGER experiment considering the same initial condition $u(0, x) = -\sin(\pi x/8)$ but $\nu = 0.01/\pi$, a condition that leads to steeper gradients. We observe that, under these settings, the oversmoothing of the predicted solution is more pronounced (see Fig. 9) thus shedding light on one of GradINN’s limitation when using a smooth prior belief to approximate a function with very steep local derivatives. This emphasizes the importance of developing methods that allows encoding more complex prior beliefs in F so as to better predict systems with discontinuities or high local gradients.

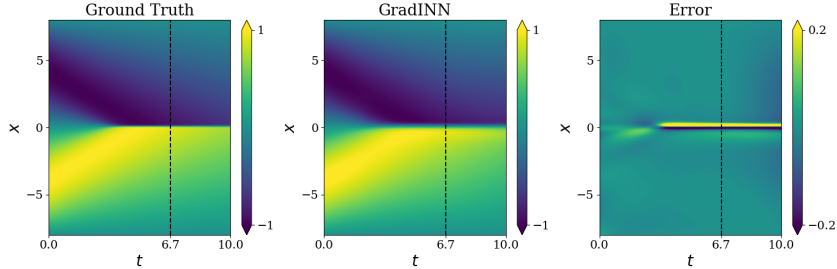


Figure 9: BURGER with $\nu = 0.01/\pi$. *Left:* GradINN predicted solution. *Middle:* Ground truth Solution. *Right:* Difference between GradINN and Ground truth.

Table 7: FRIEDMAN. RMSE_U for different values of c with $N_U = 200$ and $M = 1000$ for GradINN. For each value of c the lowest RMSE is bolded.

	$c = 0.0$	$c = 0.01$	$c = 0.03$	$c = 0.05$
s-NN	0.51	0.53	0.66	0.75
s-NN - ℓ_1	0.13	0.18	0.27	0.45
s-NN - ℓ_2	0.13	0.18	0.25	0.40
GradINN	0.04	0.07	0.19	0.30
ST	0.17	0.18	0.24	0.31

Aknowledgements

F. D. acknowledges that this study was carried out within the FAIR-Future Artificial Intelligence Research and received funding from the European Union Next-GenerationEU (PIANO NAZIONALE DI RIPRESA E RESILIENZA (PNRR)–MISSIONE 4 COMPONENTE 2, INVESTIMENTO 1.3—D.D. 1555 11/10/2022, PE00000013). This manuscript reflects only the authors’ views and opinions; neither the European Union nor the European Commission can be considered responsible for them.

References

- [1] C Basdevant, M Deville, P Haldenwang, J.M Lacroix, J Ouazzani, R Peyret, P Orlandi, and A.T Patera. Spectral and finite difference solutions of the burgers equation. *Computers & Fluids*, 14 (1):23–41, 1986. ISSN 0045-7930. doi: [https://doi.org/10.1016/0045-7930\(86\)90036-8](https://doi.org/10.1016/0045-7930(86)90036-8). URL <https://www.sciencedirect.com/science/article/pii/0045793086900368>.
- [2] Atilim Baydin, Barak Pearlmutter, Alexey Radul, and Jeffrey Siskind. Automatic differentiation in machine learning: A survey. *Journal of Machine Learning Research*, 18:1–43, 04 2018.
- [3] Alan A. Berryman. The origins and evolution of predator-prey theory. *Ecology*, 73(5):1530–1535, 1992. ISSN 00129658, 19399170. URL <http://www.jstor.org/stable/1940005>.
- [4] Shengze Cai, Zhiping Mao, Zhicheng Wang, Minglang Yin, and George Em Karniadakis. Physics-informed neural networks (pinns) for fluid mechanics: A review. *Acta Mechanica Sinica*, 37(12):1727–1738, 2021.
- [5] Shengze Cai, Zhicheng Wang, Sifan Wang, Paris Perdikaris, and George Em Karniadakis. Physics-Informed Neural Networks for Heat Transfer Problems. *Journal of Heat Transfer*, 143 (6):060801, 04 2021. ISSN 0022-1481. doi: 10.1115/1.4050542. URL <https://doi.org/10.1115/1.4050542>.
- [6] Duwon Choi, Youngkuk An, Nankyu Lee, Jinil Park, and Jonghwa Lee. Comparative study of physics-based modeling and neural network approach to predict cooling in vehicle integrated thermal management system. *Energies*, 13(20), 2020. ISSN 1996-1073. doi: 10.3390/en13205301. URL <https://www.mdpi.com/1996-1073/13/20/5301>.
- [7] Wojciech Marian Czarnecki, Simon Osindero, Max Jaderberg, Grzegorz Swirszcz, and Razvan Pascanu. Sobolev training for neural networks. *CoRR*, abs/1706.04859, 2017. URL <http://arxiv.org/abs/1706.04859>.
- [8] Jerome H Friedman. Multivariate adaptive regression splines. *The annals of statistics*, 19(1): 1–67, 1991.
- [9] Xavier Glorot and Yoshua Bengio. Understanding the difficulty of training deep feedforward neural networks. *Journal of Machine Learning Research*, 9:249–256, 2010. ISSN 15324435.
- [10] Sam Greydanus, Misko Dzamba, and Jason Yosinski. Hamiltonian neural networks, 2019.
- [11] Kurt Hornik, Maxwell Stinchcombe, and Halbert White. Multilayer feedforward networks are universal approximators. *Neural Networks*, 2(5):359–366, 1989. ISSN 0893-6080. doi: [https://doi.org/10.1016/0893-6080\(89\)90020-8](https://doi.org/10.1016/0893-6080(89)90020-8). URL <https://www.sciencedirect.com/science/article/pii/0893608089900208>.

- [12] Bin Huang and Jianhui Wang. Applications of physics-informed neural networks in power systems - a review. *IEEE Transactions on Power Systems*, 38(1):572–588, 2023. doi: 10.1109/TPWRS.2022.3162473.
- [13] Isao Ishikawa, Takeshi Teshima, Koichi Tojo, Kenta Oono, Masahiro Ikeda, and Masashi Sugiyama. Universal approximation property of invertible neural networks. *Journal of Machine Learning Research*, 24(287):1–68, 2023. URL <http://jmlr.org/papers/v24/22-0384.html>.
- [14] George Karniadakis, Yannis Kevrekidis, Lu Lu, Paris Perdikaris, Sifan Wang, and Liu Yang. Physics-informed machine learning. pages 1–19, 05 2021. doi: 10.1038/s42254-021-00314-5.
- [15] Diederik P. Kingma and Jimmy Ba. Adam: A method for stochastic optimization. In Yoshua Bengio and Yann LeCun, editors, *3rd International Conference on Learning Representations, ICLR 2015, San Diego, CA, USA, May 7-9, 2015, Conference Track Proceedings*, 2015. URL <http://arxiv.org/abs/1412.6980>.
- [16] Zhiping Mao, Ameya D. Jagtap, and George Em Karniadakis. Physics-informed neural networks for high-speed flows. *Computer Methods in Applied Mechanics and Engineering*, 360:112789, 2020. ISSN 0045-7825. doi: <https://doi.org/10.1016/j.cma.2019.112789>. URL <https://www.sciencedirect.com/science/article/pii/S0045782519306814>.
- [17] Marios Mattheakis, David Sondak, Akshunna S. Dogra, and Pavlos Protopapas. Hamiltonian neural networks for solving equations of motion. *Physical Review E*, 105(6), June 2022. ISSN 2470-0053. doi: 10.1103/physreve.105.065305. URL <http://dx.doi.org/10.1103/PhysRevE.105.065305>.
- [18] Miquel Noguer i Alonso and Daniel Maxwell. Physics-informed neural networks (pinns) in finance. *Daniel, Physics-Informed Neural Networks (PINNs) in Finance (October 10, 2023)*, 2023.
- [19] S. Oreški. Comparison of neural network and empirical models for prediction of second virial coefficients for gases. *Procedia Engineering*, 42:303–312, 2012. ISSN 1877-7058. doi: <https://doi.org/10.1016/j.proeng.2012.07.421>. URL <https://www.sciencedirect.com/science/article/pii/S1877705812028214>. CHISA 2012.
- [20] Philipp Pilar and Niklas Wahlström. Physics-informed neural networks with unknown measurement noise, 2023.
- [21] Allan Pinkus. Approximation theory of the mlp model in neural networks. *Acta Numerica*, 8: 143–195, 1999. doi: 10.1017/S0962492900002919.
- [22] Lena Podina, Brydon Eastman, and Mohammad Kohandel. Universal physics-informed neural networks: symbolic differential operator discovery with sparse data. In *Proceedings of the 40th International Conference on Machine Learning, ICML'23*. JMLR.org, 2023.
- [23] M. Raissi, P. Perdikaris, and G.E. Karniadakis. Physics-informed neural networks: A deep learning framework for solving forward and inverse problems involving nonlinear partial differential equations. *Journal of Computational Physics*, 378:686–707, 2019. ISSN 0021-9991. doi: <https://doi.org/10.1016/j.jcp.2018.10.045>. URL <https://www.sciencedirect.com/science/article/pii/S0021999118307125>.
- [24] Maziar Raissi. Deep hidden physics models: Deep learning of nonlinear partial differential equations. *Journal of Machine Learning Research*, 19, 01 2018.
- [25] Junuthula Narasimha Reddy. *An introduction to the finite element method*, volume 3. McGraw-Hill New York, 2013.
- [26] Nilanjan Saha, Aleena Swetapadma, and Mahadev Mondal. A brief review on artificial neural network: Network structures and applications. In *2023 9th International Conference on Advanced Computing and Communication Systems (ICACCS)*, volume 1, pages 1974–1979, 2023. doi: 10.1109/ICACCS57279.2023.10112753.

- [27] Hwijae Son, Jin Woo Jang, Woo Jin Han, and Hyung Ju Hwang. Sobolev training for physics informed neural networks. *arXiv preprint arXiv:2101.08932*, 2021.
- [28] Sir George Gabriel Stokes. On the effect of the internal friction of fluids on the motion of pendulums. *From the Transactions of the Cambridge Philosophical Society, Vol. IX. p. [8]*, 18, 12 1850.
- [29] Jeremy Yu, Lu Lu, Xuhui Meng, and George Em Karniadakis. Gradient-enhanced physics-informed neural networks for forward and inverse pde problems. *Computer Methods in Applied Mechanics and Engineering*, 393:114823, 2022. ISSN 0045-7825. doi: <https://doi.org/10.1016/j.cma.2022.114823>. URL <https://www.sciencedirect.com/science/article/pii/S0045782522001438>.